Thermodynamics of the NJL model at finite isospin chemical potential

Bachelor-Thesis von Lennart Kurth
Tag der Einreichung:

1. Gutachten: Priv. Doz. Dr. Michael Buballa
2. Gutachten: Prof. Ph.D. Guy Moore

TECHNISCHE UNIVERSITÄT DARMSTADT

Fachbereich Physik
Institut für Kernphysik
Nuclei, Hadrons and Quarks

Thermodynamics of the NJL model at finite isospin chemical potential

Vorgelegte Bachelor-Thesis von Lennart Kurth

1. Gutachten: Priv. Doz. Dr. Michael Buballa
2. Gutachten: Prof. Ph.D. Guy Moore

Tag der Einreichung:

Erklärung zur Bachelor-Thesis

Hiermit versichere ich, die vorliegende Bachelor-Thesis ohne Hilfe Dritter nur mit den angegebenen Quellen und Hilfsmitteln angefertigt zu haben. Alle Stellen, die aus Quellen entnommen wurden, sind als solche kenntlich gemacht. Diese Arbeit hat in gleicher oder ähnlicher Form noch keiner Prüfungsbehörde vorgelegen.

Darmstadt, den 28.12.2017

(Lennart Kurth)

Abstract

In this bachelor's thesis we analyze strongly interacting matter under certain conditions. These are vanishing baryon chemical potential, finite isospin chemical potential and finite temperature. Further, we take only two flavors with identical bare quark mass into account. For our calculations we use the Nambu–Jona-Lasinio model in mean field approximation and consider sigma and pion condensation. Through minimization of the grand potential we obtain pressure, isospin density and energy density. We also compare our results to the previous works [3] and [1], where different methods have been used.

Contents

List of Figures

1 Introduction

We want to analyze the properties of strongly interacting matter, which is described by quantum chromodynamics (QCD), a part of the standard model. This interaction couples to color charged particles and is mediated by gluons. Both quarks and gluons themselves are color charged. This leads to the complexity emerging from the strong interaction. For example only color neutral particles are observed, a fact called confinement. Although quantum chromodynamics is believed to describe the strong interaction correctly, it is difficult to directly calculate predictions from it. Perturbation theory can only be applied at large energies due to the large coupling constant at low energies. Furthermore the symmetry group it is based on, SU(3), is non-abelian. With increasing computational power, the theory can be evaluated numerically on a discretized spacetime, a method called lattice QCD. This method is however only applicable if the baryon chemical potential vanishes.
To evaluate a system containing a large number of degrees of freedom, statistical physics is applied. Its results can be visualized in a phase diagram. In figure 1.1 a qualitative picture of the phase diagram of QCD is drawn. It shows the different phases of strongly interacting matter for two flavors with vanishing bare quark mass depending on baryon chemical potential and temperature. At low temperature and baryon chemical potential the quarks and gluons are confined in hadrons. There is a first order phase transition, that means non-continuous transition, from this phase to the deconfined phase at low temperatures and large enough baryon chemical potential. This phase is called the quark-gluon plasma (QGP). In the case shown in the figure there is also a second order phase transition, that means non-differentiable transition, at small baryon chemical potential and large enough temperatures. The point where these two phase transitions meet is called tricritical point. If we instead consider two flavors with finite bare quark mass, as we do in this thesis, the first order phase transition ends in a critical endpoint and the second order phase transition is replaced by a crossover. As mentioned above it is so far not possible to derive these properties from QCD directly. The phases and their boundaries, especially the first order phase transition and its endpoint, are results of simplifying models and hence speculative. The crossover can be confirmed by lattice QCD at zero baryon chemical potential.
To get predictions on strongly interacting matter at low energies, despite the difficulties with quantum chromodynamics, simplifying models can be used. Their predictions can then be compared for specific regions and parameters. If predictions of different models match it increases their significance. Especially lattice QCD results can validate other models in certain regions. Conversely these models my be used to make predictions about regions not accessible to lattice QCD. It turns out, that lattice QCD can be applied to systems with vanishing baryon chemical potential but finite isospin chemical potential. The chemical potential describes the change in energy for varying particle number. Therefore the isospin chemical potential describes the change in energy that is caused by the difference between the number of up quarks and down quarks. This particular case is only of theoretical interest, since such conditions are not found in nature. Inside of neutron stars the isospin chemical potential and baryon chemical potential are both finite.

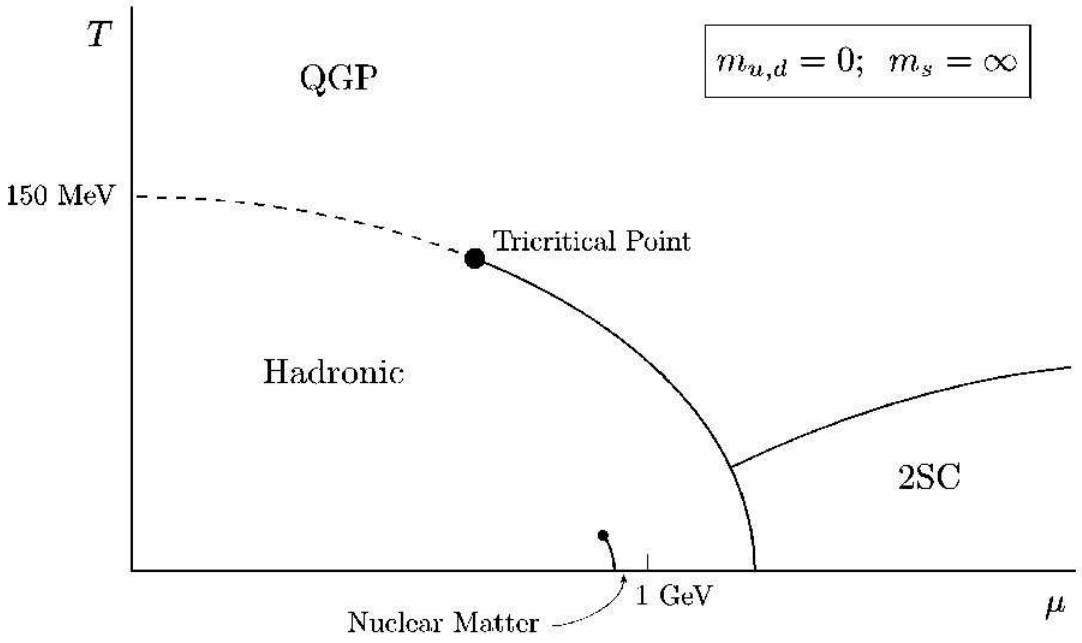

Figure 1.1: QCD phase diagram taken from [6]

As a simplifying model to work with we choose the Nambu–Jona-Lasinio (NJL) model [5]. It was first introduced to describe nucleons and is now used as an approximation for quantum chromodynamics. In this model gluons are replaced by a four point quark interaction. This makes the model simpler and predictions can be made about regions not accessible with QCD. On the downside, it does not describe correctly the physics at small scales and high energies. Within the NJL model it is possible to calculate predictions for finite baryon chemical potential as well as for finite isospin chemical potential. This way we can compare the results at finite isospin chemical potential and test the validity of the NJL model. One example for a comparable result is the so called pion condensation. It is predicted to emerge at large enough isospin chemical potential by lattice QCD and can also be described by the NJL model. These lattice calculations have been performed by [1] and others. Another example is the analysis of thermodynamic properties of strongly interacting matter. In particular we will calculate pressure, isospin density and energy density. We will compare our zero temperature results to [3], where analytic expressions have been derived via an effective theory, chiral perturbation theory (χPT). In short it is our goal to compare the predictions made by the Nambu–Jona-Lasinio model with those made by lattice QCD and chiral perturbation theory. We focus on the case that the baryon chemical potential is zero but there is a difference in the chemical potential for up and down quarks, because only here lattice QCD is applicable.

2 Calculations

2.1 Mean field approximation

The concrete Lagrangian we use, given by the Nambu–Jona-Lasinio model, is

$$\mathcal{L} = \bar{\psi}(i\partial\!\!\!/ - m)\psi + G((\bar{\psi}\psi)^2 + (\bar{\psi}i\gamma_5\vec{\tau}\psi)^2) \; .$$

Further, we assume only two quark flavors, up u and down d, such that $\psi = (u, d)^T$ and $m = \mathrm{diag}(m_u, m_d)$. $\vec{\tau}$ are the Pauli matrices in isospin space. Then the Lagrangian, expressed as a function of u and d, is

$$\begin{aligned}\mathcal{L} = \bar{u}(i\partial\!\!\!/ - m_u)u + \bar{d}(i\partial\!\!\!/ - m_d)d + G(\bar{u}u + \bar{d}d)^2 \\ + G(\bar{u}i\gamma_5 u - \bar{d}i\gamma_5 d)^2 + 4G(\bar{u}i\gamma_5 d)(\bar{d}i\gamma_5 u)) \; .\end{aligned}$$

Now we conduct a mean field approximation, that means we expand the Lagrangian linearly around the expectation values of $\bar{\psi}\psi$ and $\bar{\psi}i\gamma_5\vec{\tau}\psi$. We substitute

$$\begin{aligned}\bar{\psi}\psi &= \langle\bar{\psi}\psi\rangle + \delta(\bar{\psi}\psi) \; , \\ \bar{\psi}i\gamma_5\vec{\tau}\psi &= \langle\bar{\psi}i\gamma_5\vec{\tau}\psi\rangle + \delta(\bar{\psi}i\gamma_5\vec{\tau}\psi) \; .\end{aligned}$$

These expressions only appear squared and the resulting $\delta(\bar{\psi}\psi)^2$ and $\delta(\bar{\psi}i\gamma_5\vec{\tau}\psi)^2$ are omitted. The remaining δ terms can be written in terms of the original expression. This leads to

$$\begin{aligned}(\bar{\psi}\psi)^2 &= 2\langle\bar{\psi}\psi\rangle(\bar{\psi}\psi) - \langle\bar{\psi}\psi\rangle^2 \; , \\ (\bar{\psi}i\gamma_5\vec{\tau}\psi)^2 &= 2\langle\bar{\psi}i\gamma_5\vec{\tau}\psi\rangle(\bar{\psi}i\gamma_5\vec{\tau}\psi) - \langle\bar{\psi}i\gamma_5\vec{\tau}\psi\rangle^2 \; .\end{aligned}$$

$\langle\bar{\psi}\psi\rangle$ is interpreted as the sigma condensate σ and $\langle\bar{\psi}i\gamma_5\vec{\tau}\psi\rangle$ as the pion condensate $\vec{\pi} = (\pi_1, \pi_2, \pi_3)$. This way $\mathcal{L}$ can be written as

$$\mathcal{L} = \bar{\psi}(i\partial\!\!\!/ - m)\psi + \bar{\psi}(2G\sigma)\psi + \bar{\psi}(2Gi\gamma_5\vec{\tau}\cdot\vec{\pi})\psi - G(\sigma^2 + \vec{\pi}^2) \; .$$

Now the interaction parts are of the form $\bar{\psi}\psi$ times a constant and thus can be absorbed in an effective mass term M. With

$$M = m - 2G(\sigma + i\gamma_5\vec{\tau}\cdot\vec{\pi})$$

we get a Lagrangian that resembles the Lagrangian of free fermions plus a constant term

$$\mathcal{L} = \bar{\psi}(i\partial\!\!\!/ - M)\psi - G(\sigma^2 + \vec{\pi}^2) \; .$$

Note that M is not diagonal and the two flavors do not decouple. The Lagrangian is therefore more complex than the one for free fermions.

2.2 Chemical potential

We are only interested in the case that the baryon chemical potential vanishes

$$\mu_B = \frac{3}{2}(\mu_u + \mu_d) = 0 \ .$$

μ_u and μ_d are the chemical potential for the up and down quarks respectively. The isospin chemical potential is defined as

$$\mu_I = 2\Delta\mu = (\mu_u - \mu_d) \ .$$

Thus $\mu_u = \Delta\mu$ and $\mu_d = -\Delta\mu$.

2.3 Grand potential

The partition function $\mathcal{Z}$ is defined as

$$\mathcal{Z} = \mathrm{Tr}\left[\exp\left(-\beta \int \mathrm{d}^3x(\mathcal{H} - \psi^\dagger \mu \psi)\right)\right]$$

with the Hamiltonian density $\mathcal{H}$ and $\mu = \mathrm{diag}(\mu_u, \mu_d)$. By a long calculation [4] which we do not carry out here, it can be shown that

$$\begin{aligned}\mathcal{Z} =& \exp(-\beta V G(\sigma^2 + \vec{\pi}^2)) \\ &\times \exp\left(2n_c V \int \frac{\mathrm{d}^3p}{(2\pi)^3}(\beta E_+ + \beta E_- + 2\ln(1+\exp(-\beta E_+)) + 2\ln(1+\exp(-\beta E_-))\right) ,\end{aligned}$$

where n_c is the color degeneracy and

$$E_\pm = \sqrt{\left(\sqrt{\vec{p}^2 + (2G\sigma - m)^2 + (2G\pi_3)^2} \pm \Delta\mu\right)^2 + (2G\pi_1)^2 + (2G\pi_2)^2} \ .$$

From this the grand potential Ω can be obtained by

$$\Omega = -\frac{1}{\beta V}\log \mathcal{Z} \ .$$

We get the grand potential describing the system in mean field approximation

$$\begin{aligned}\Omega =& G(\sigma^2 + \vec{\pi}^2) - 2n_c \int \frac{\mathrm{d}^3p}{(2\pi)^3}(E_+ + E_-) \\ &- 2n_c \int \frac{\mathrm{d}^3p}{(2\pi)^3}\frac{2}{\beta}\left(\ln(1+\exp(-\beta E_+)) + \ln(1+\exp(-\beta E_-))\right) \ .\end{aligned}$$

Its first integral is divergent. We solve this problem by applying a momentum cutoff. Our model is not renormalizable and the cutoff is chosen to reproduce observables of the pion, as described in section 3.1.
With the grand potential we can calculate the sigma and pion condensate at given isospin chemical potential $\Delta\mu$ and temperature T. The ground state is at the global minimum of the grand potential which must therefore be minimized. Calculating the derivative and setting it zero yields the gap equation, which must be solved.

2.4 Gap equation

The solution to the gap equation is not unique and the values of the grand potential must be compared for all solutions, to find the global minimum. The grand potential only depends on σ, $\pi_3 =: \pi_0$ and $\sqrt{\pi_1^2+\pi_2^2} =: \pi_\pm$. Thus the gap equation is a system of three equations. These equations are

$$0 \stackrel{!}{=} \frac{\partial\Omega}{\partial\sigma} = 2G\sigma - \frac{n_c}{\pi^2}\int_0^\Lambda \mathrm{d}p p^2 \left(\frac{\partial E_+}{\partial\sigma} + \frac{\partial E_-}{\partial\sigma}\right) + \frac{n_c}{\pi^2}\int_0^\infty \mathrm{d}p p^2 \left(\frac{\partial E_+}{\partial\sigma}\frac{2}{1+\exp(-\beta E_+)} + \frac{\partial E_-}{\partial\sigma}\frac{2}{1+\exp(-\beta E_-)}\right), \tag{2.1}$$

$$0 \stackrel{!}{=} \frac{\partial\Omega}{\partial\pi_0} = 2G\pi_0 - \frac{n_c}{\pi^2}\int_0^\Lambda \mathrm{d}p p^2 \left(\frac{\partial E_+}{\partial\pi_0} + \frac{\partial E_-}{\partial\pi_0}\right) + \frac{n_c}{\pi^2}\int_0^\infty \mathrm{d}p p^2 \left(\frac{\partial E_+}{\partial\pi_0}\frac{2}{1+\exp(-\beta E_+)} + \frac{\partial E_-}{\partial\pi_0}\frac{2}{1+\exp(-\beta E_-)}\right), \tag{2.2}$$

$$0 \stackrel{!}{=} \frac{\partial\Omega}{\partial\pi_\pm} = 2G\pi_\pm - \frac{n_c}{\pi^2}\int_0^\Lambda \mathrm{d}p p^2 \left(\frac{\partial E_+}{\partial\pi_\pm} + \frac{\partial E_-}{\partial\pi_\pm}\right) + \frac{n_c}{\pi^2}\int_0^\infty \mathrm{d}p p^2 \left(\frac{\partial E_+}{\partial\pi_\pm}\frac{2}{1+\exp(-\beta E_+)} + \frac{\partial E_-}{\partial\pi_\pm}\frac{2}{1+\exp(-\beta E_-)}\right). \tag{2.3}$$

The derivatives of $E_\pm$ are

$$\frac{\partial E_\pm}{\partial\sigma} = 2G\frac{2G\sigma - m}{E_\pm}\left(1 \pm \frac{\Delta\mu}{\sqrt{\vec{p}^2 + (2G\sigma - m)^2 + (2G\pi_0)^2}}\right),$$

$$\frac{\partial E_\pm}{\partial\pi_0} = 2G\frac{2G\pi_0}{E_\pm}\left(1 \pm \frac{\Delta\mu}{\sqrt{\vec{p}^2 + (2G\sigma - m)^2 + (2G\pi_0)^2}}\right),$$

$$\frac{\partial E_\pm}{\partial\pi_\pm} = 2G\frac{2G\pi_\pm}{E_\pm}.$$

We observe that the integral parts of equation 2.1 and equation 2.2 only differ by factors of $2G\sigma - m$ and $2G\pi_0$. Adding and subtracting m from equation 2.1 allows us to rewrite both equations as

$$0 \stackrel{!}{=} \frac{\partial \Omega}{\partial \sigma} = m + (2G\sigma - m)f \ , \tag{2.4}$$

$$0 \stackrel{!}{=} \frac{\partial \Omega}{\partial \pi_0} = 2G\pi_0 f \ , \tag{2.5}$$

where

$$f = 1 - 2G\frac{n_c}{\pi^2}\int_0^\Lambda \mathrm{d}p p^2 \left(\frac{1+g}{E_+} + \frac{1-g}{E_-}\right)$$
$$+ 2G\frac{n_c}{\pi^2}\int_0^\infty \mathrm{d}p p^2 \left(\frac{1+g}{E_+}\frac{2}{1+\exp(-\beta E_+)} + \frac{1-g}{E_-}\frac{2}{1+\exp(-\beta E_-)}\right)$$

and

$$g = \frac{\Delta\mu}{\sqrt{\vec{p}^2 + (2G\sigma - m)^2 + (2G\pi_0)^2}} \ .$$

Now we can use that $m > 0$ and conclude from equation 2.4 that $f \neq 0$. Then it follows from equation 2.5 that $\pi_0 = 0$. Since π_0 is always zero, if the gap equation is fulfilled, the system of equations can be reduced to two equations of two variables

$$0 \stackrel{!}{=} \frac{\partial \Omega}{\partial \sigma} = 2G\sigma - \frac{n_c}{\pi^2}\int_0^\Lambda \mathrm{d}p p^2 \left(\frac{\partial \tilde{E}_+}{\partial \sigma} + \frac{\partial \tilde{E}_-}{\partial \sigma}\right)$$
$$+ \frac{n_c}{\pi^2}\int_0^\infty \mathrm{d}p p^2 \left(\frac{\partial \tilde{E}_+}{\partial \sigma}\frac{2}{1+\exp(-\beta \tilde{E}_+)} + \frac{\partial \tilde{E}_-}{\partial \sigma}\frac{2}{1+\exp(-\beta \tilde{E}_-)}\right) ,$$

$$0 \stackrel{!}{=} \frac{\partial \Omega}{\partial \pi_\pm} = 2G\pi_\pm - \frac{n_c}{\pi^2}\int_0^\Lambda \mathrm{d}p p^2 \left(\frac{\partial \tilde{E}_+}{\partial \pi_\pm} + \frac{\partial \tilde{E}_-}{\partial \pi_\pm}\right)$$
$$+ \frac{n_c}{\pi^2}\int_0^\infty \mathrm{d}p p^2 \left(\frac{\partial \tilde{E}_+}{\partial \pi_\pm}\frac{2}{1+\exp(-\beta \tilde{E}_+)} + \frac{\partial \tilde{E}_-}{\partial \pi_\pm}\frac{2}{1+\exp(-\beta \tilde{E}_-)}\right) .$$

The new variables

$$\tilde{E}_\pm = \sqrt{\left(\sqrt{\vec{p}^2 + (2G\sigma - m)^2} \pm \Delta\mu\right)^2 + (2G\pi_\pm)^2}$$

and their derivatives

$$\frac{\partial \tilde{E}_\pm}{\partial \sigma} = 2G\frac{2G\sigma - m}{\tilde{E}_\pm}\left(1 \pm \frac{\Delta\mu}{\sqrt{\vec{p}^2 + (2G\sigma - m)^2}}\right),$$

$$\frac{\partial \tilde{E}_\pm}{\partial \pi_\pm} = 2G\frac{2G\pi_\pm}{\tilde{E}_\pm}$$

no longer depend on π_0. We did not attempt to solve the gap equation analytically. All further results are obtained by numerical methods. Specifically we used the *fsolve* and *fmin* routine provided in SciPy for the Python programming language. Note, that the first routine is not enough, because a solution to the gap equation can also be a maximum or saddle point of the grand potential. We therefore visually analyzed the global behavior of Ω and used the algorithms with appropriate starting points.

2.5 Thermodynamic quantities

We can derive all thermodynamic quantities from the partition function and therefore from the grand potential. Here we calculate the pressure, the isospin density and the energy density using the following thermodynamic relations. To normalize the pressure and energy density in vacuum to zero, we subtract Ω_0, the grand potential at $T = \Delta\mu = 0$, from the grand potential everywhere. Changing the grand potential by a global constant does not change physics.

$$p = -(\Omega - \Omega_0)$$

$$n_I = -\frac{\partial \Omega}{\partial \mu_I}$$

$$\epsilon = -p - \frac{\partial \Omega}{\partial T}T - \frac{\partial \Omega}{\partial \mu_I}\mu_I$$

The grand potential is evaluated at its global minimum with respect to the condensates. Pressure, isospin density and energy density therefore only depend on the temperature T and the isospin chemical potential $\Delta\mu$. The resulting dependencies are presented in the next chapter.

3 Results

3.1 Parameters

We set the same mass $m_u = m_d = m = 5.6\,\text{MeV}$ for up and down quarks. The momentum cutoff is chosen as $\Lambda = 587.9\,\text{MeV}$. The coupling constant of our Lagrangian is set to $G = 2.44/\Lambda^2$. These three parameters have been taken from [2]. Together they produce a physical pion mass $m_\pi = 135\,\text{MeV}$ and pion decay constant $f_\pi = 92.4\,\text{MeV}$. Furthermore the color degeneracy is $n_c = 3$, since there are three types of color charge.

3.2 Condensates

In figure 3.1 and figure 3.2 the pion condensate is shown, scaled with a factor of $2G$. Pion condensate from here on always means the condensate of $\pi_\pm$, since for π_0 no condensation occurs. Figure 3.3 and figure 3.4 show the scaled sigma condensate respectively. At an isospin chemical potential smaller than the mass of the pion, $\Delta\mu < m_\pi/2$, the pion condensate is zero. This is expected, since the difference of μ_u and $-\mu_d$ is $2\Delta\mu < m_\pi$. The sigma condensate is negative and constant at vanishing temperatures. Its value is slightly larger than $-400\,\text{MeV}/2G$. We first look at the behavior at $T = 0$. Both, sigma and pion condensate, show a rapid increase when the isospin chemical potential is increased to $\Delta\mu > m_\pi/2$. The sigma condensate goes asymptotically to a value smaller than zero, since we chose a finite bare quark mass. The pion condensate shows a similar growth and goes asymptotically to $400\,\text{MeV}/2G$.
At $T > 0$ the phase transition at small temperature remains the same for both condensates. Around $T = 100\,\text{MeV}$ the phase transition for the pion condensate starts shifting towards larger isospin chemical potential. The sigma condensate goes to its maximal value, which is negative, as the temperature increases, at first slowly, than faster. Also the shift of the phase transition to larger $\Delta\mu$ for increasing T appears as it did for the pion condensate. Unlike the pion condensate, the sigma condensate at finite $\Delta\mu$ drops for small T to smaller values before it starts growing again at larger T. It does however always grow with $\Delta\mu$.
A special property of the sigma and pion condensate is highlighted in figure 3.5. Adding together the squares of both condensates at low temperatures results in a nearly constant function of $\Delta\mu$. The square root of this quantity can be interpreted as the length of a vector in the σ-$\pi_\pm$-plane. When the isospin chemical potential changes this vector rotates, but does not change its length. At higher temperatures this property is lost, since both condensates ultimately go to zero.

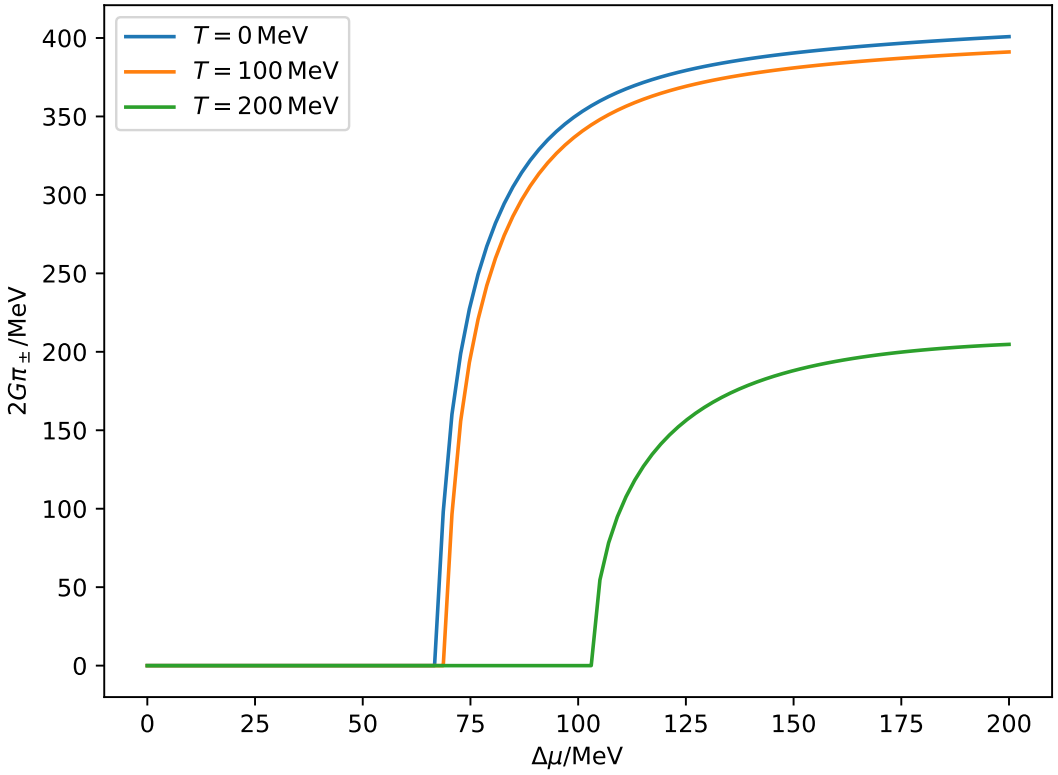

Figure 3.1: Pion condensate against $\Delta\mu$ at different T

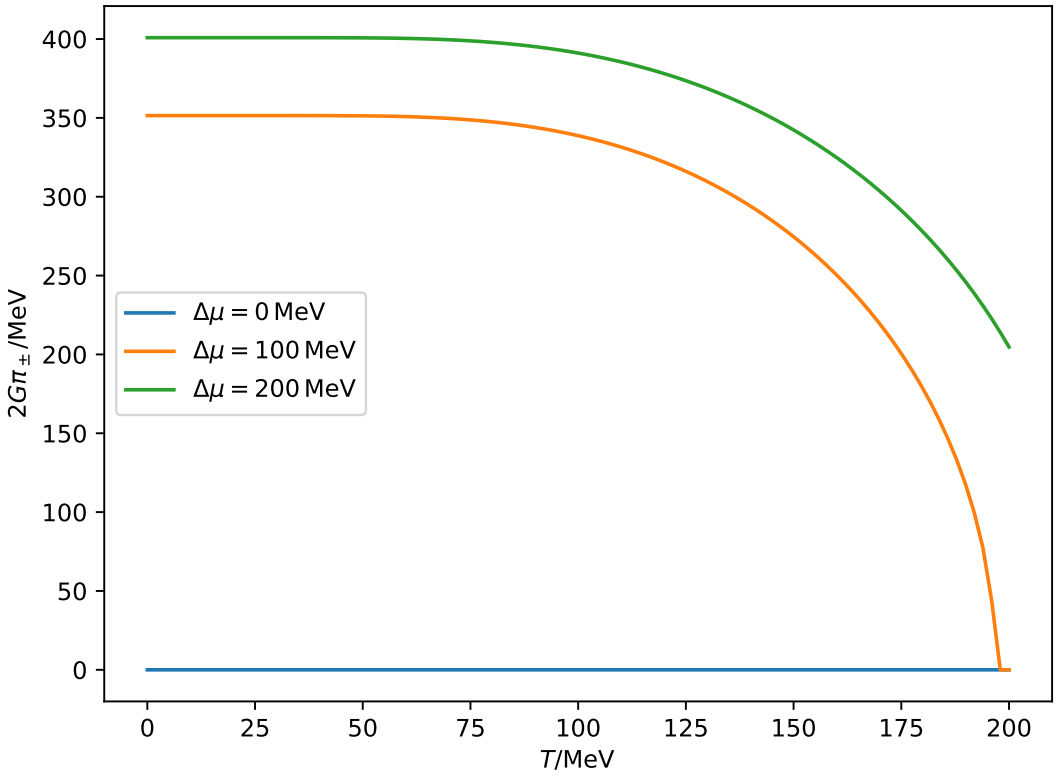

Figure 3.2: Pion condensate against T at different $\Delta\mu$

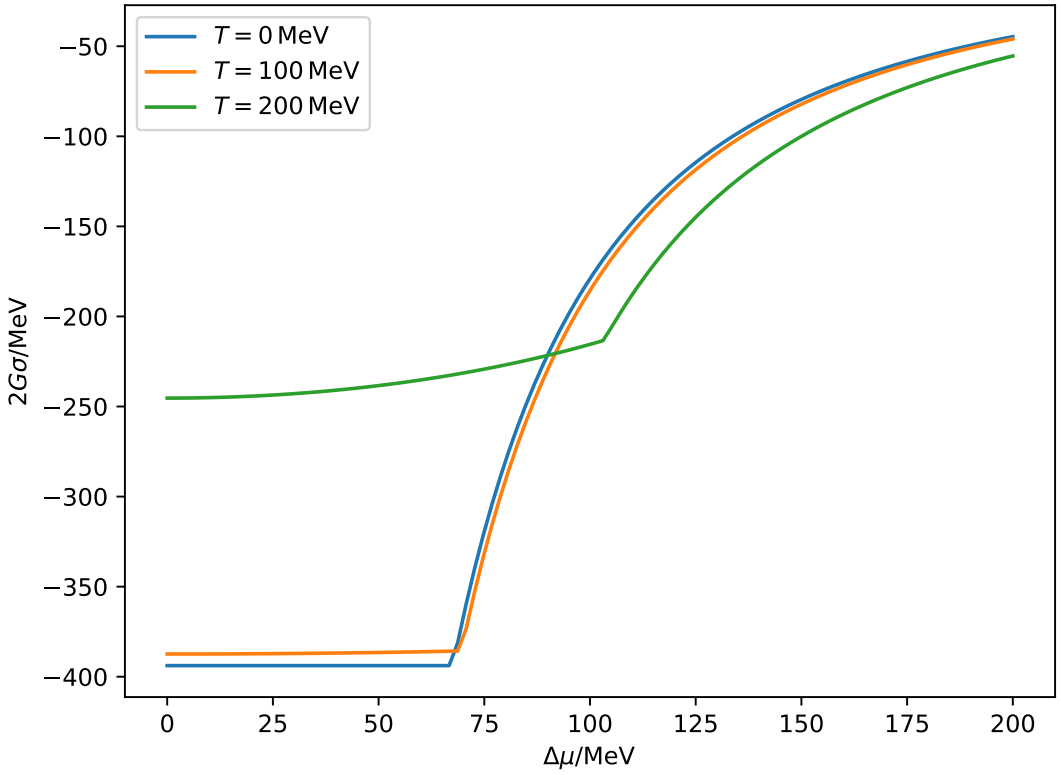

Figure 3.3: Sigma condensate against $\Delta\mu$ at different T

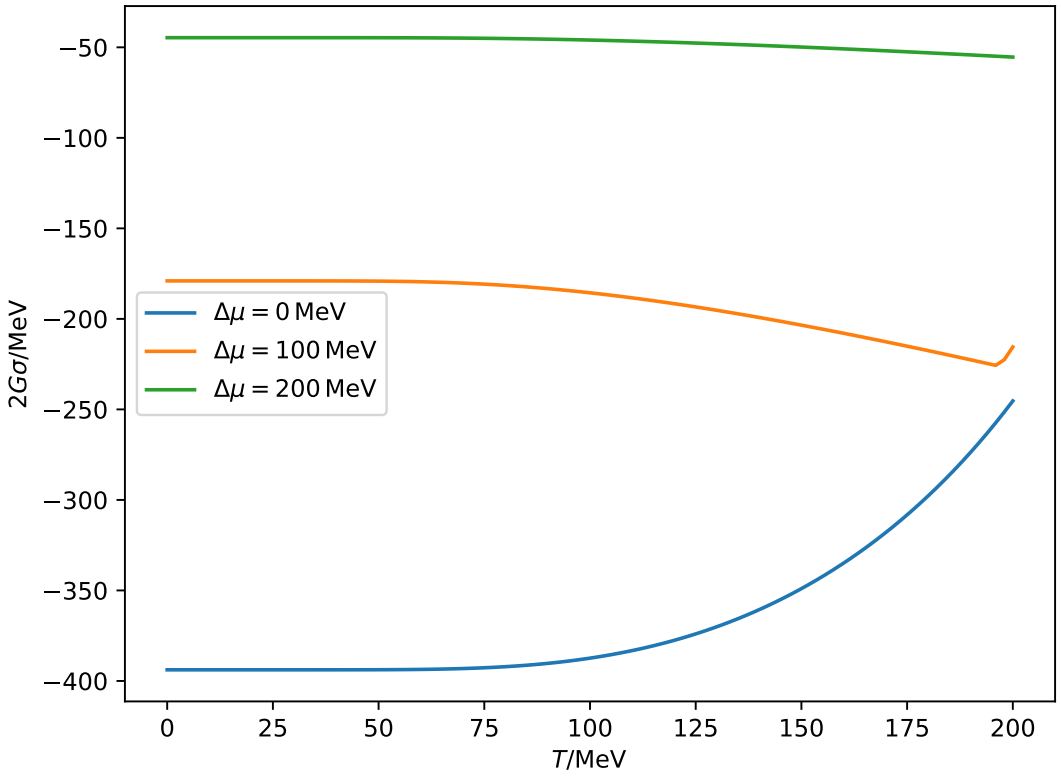

Figure 3.4: Sigma condensate against T at different $\Delta\mu$

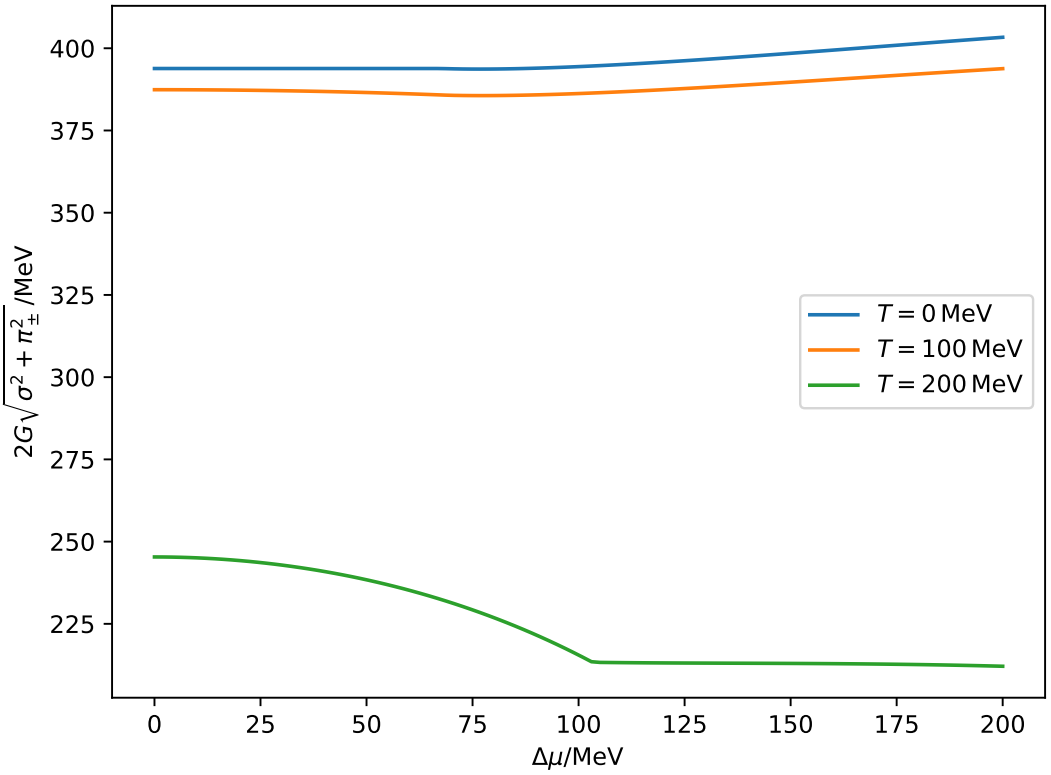

Figure 3.5: Combination of sigma and pion condensate against $\Delta\mu$ at $T = 0$

3.3 Pressure

The pressure dependence on T and $\Delta\mu$ can be seen in figure 3.6 and figure 3.7. Since the pressure p is just $-\Omega$, its value at a given point in the phase diagram is the negative of the global minimum of the grand potential at this point. The pressure increases when the isospin chemical potential or the temperature are increased. For this reason, p remains greater than zero. The pressure grows faster with temperature than it does with isospin chemical potential. At zero temperature the pressure only starts growing for $\Delta\mu > m_\pi/2$.

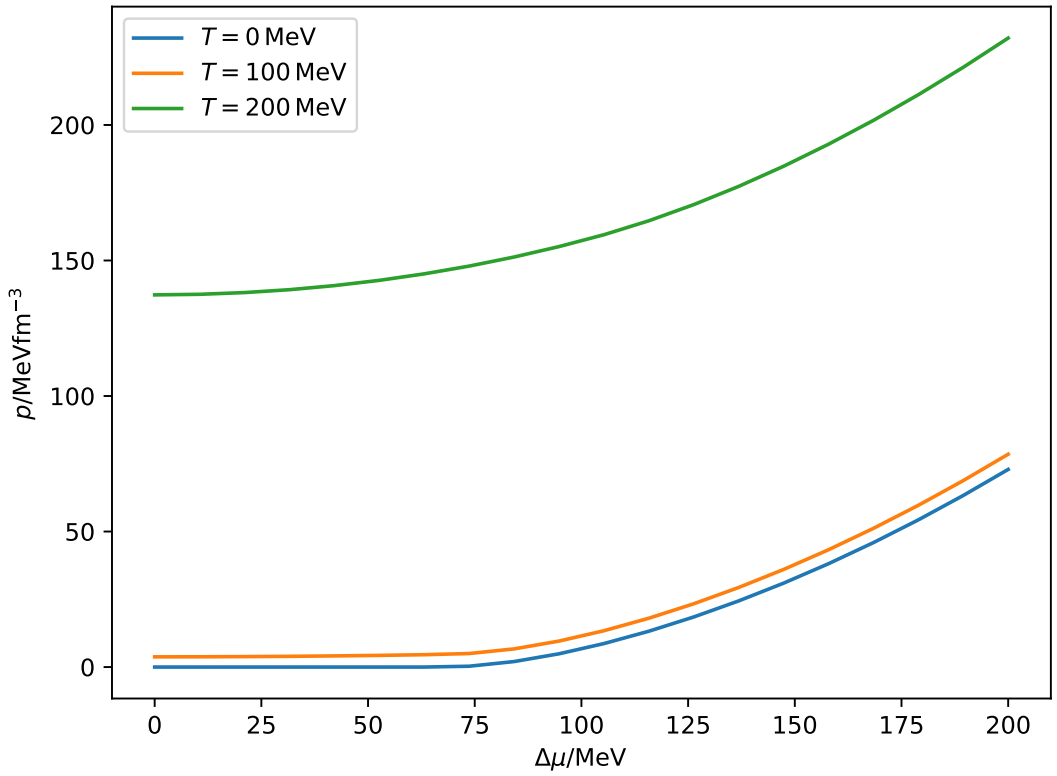

Figure 3.6: Pressure against $\Delta\mu$ at different T

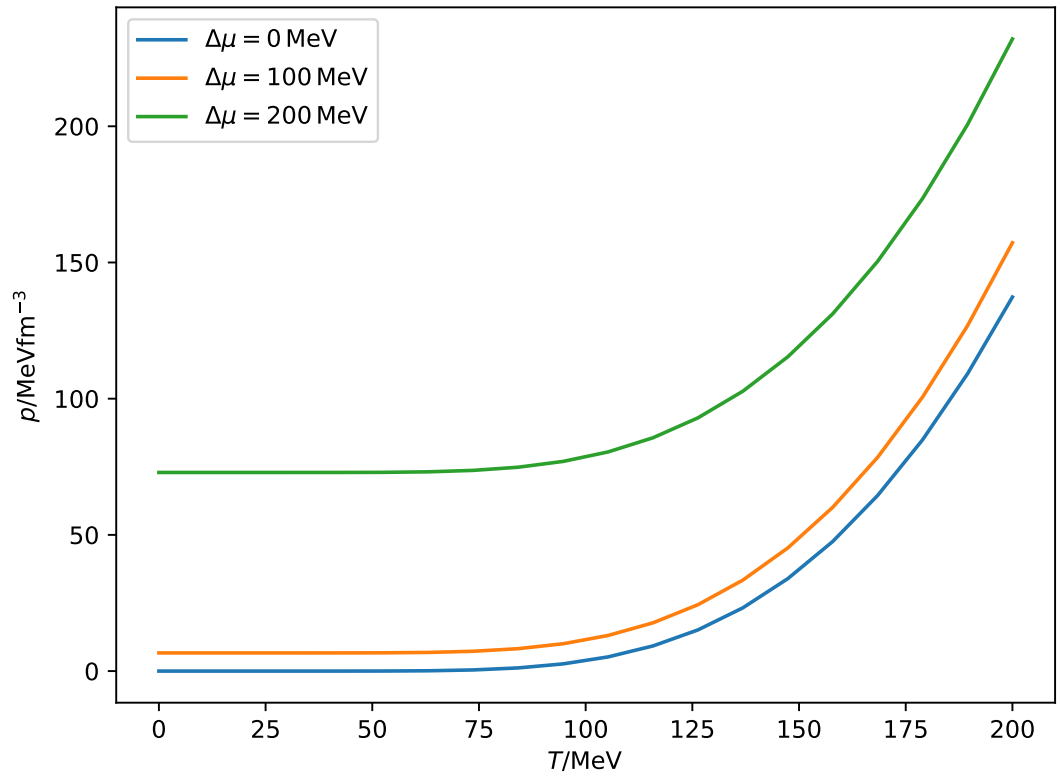

Figure 3.7: Pressure against T at different $\Delta\mu$

3.4 Isospin density

At zero temperature the isospin density n_I vanishes until $\Delta\mu > m_\pi/2$, analogous to the pion condensate. Above this point the isospin density starts growing asymptotically linear with $\Delta\mu$. For $T > 0$ and vanishing isospin chemical potential the isospin density is also zero. But now at finite $\Delta\mu$ there is always $n_I > 0$. The finite temperature makes pion creation and hence a finite isospin density possible, even at $\Delta\mu < m_\pi/2$. For temperatures larger than about 200 MeV the isospin density grows linearly with the isospin chemical potential. We show the isospin density dependence on T and $\Delta\mu$ in figure 3.8 and figure 3.9.

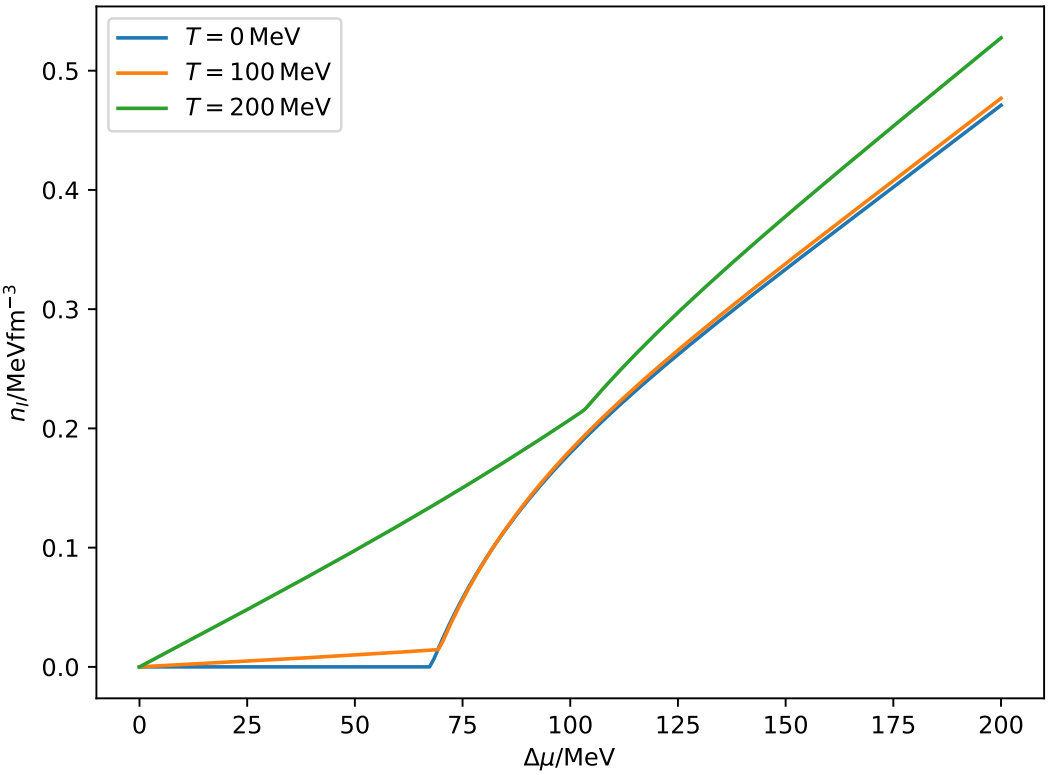

Figure 3.8: Isospin density against $\Delta\mu$ at different T

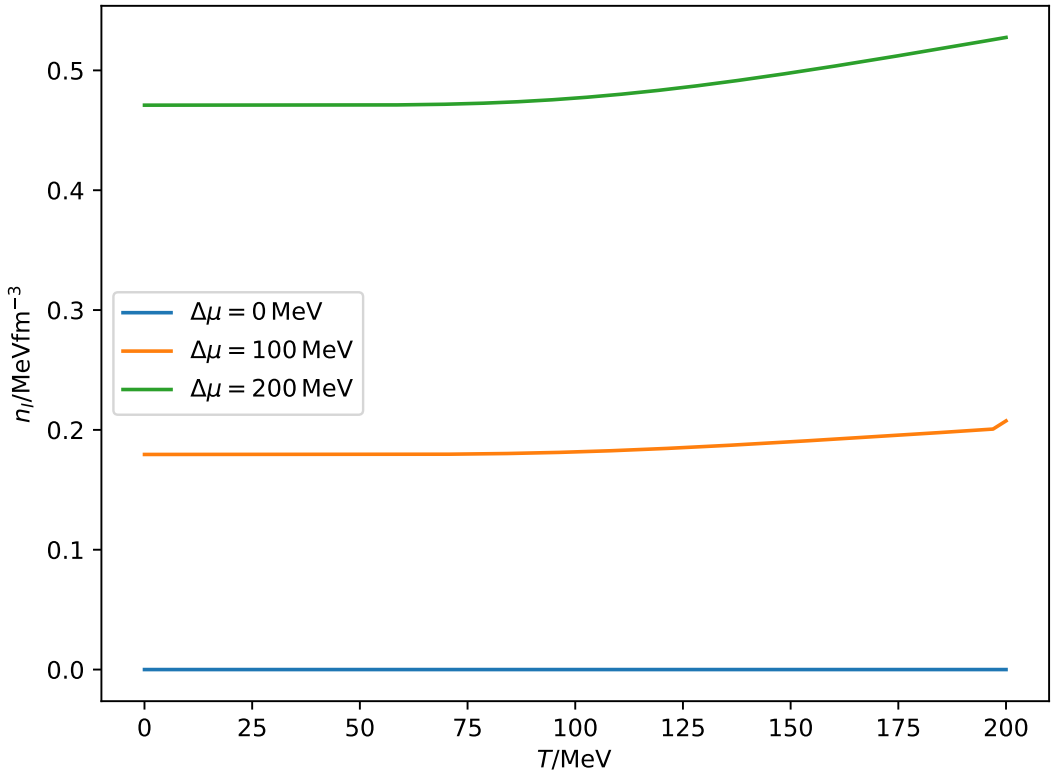

Figure 3.9: Isospin density against T at different $\Delta\mu$

3.5 Energy density

The energy density is shown in figure 3.10 and figure 3.11. For vanishing temperature it is zero up to an isospin chemical potential of $\Delta\mu = m_\pi/2$. From there it grows asymptotically linear with $\Delta\mu$. At low temperatures the behavior for $\Delta\mu > m_\pi/2$ stays the same. For $\Delta\mu < m_\pi/2$ and finite temperature the energy density does not vanish, analogous to the isospin density. Unlike the isospin density the energy density is not zero for finite $\Delta\mu$. The growth of the energy density with temperature is comparable to that of the pressure and begins likewise around 80 MeV. At $T = 200$ MeV there is still a small bump in figure 3.10. This is a remainder of the transition from $\Delta\mu < m_\pi/2$ to $\Delta\mu > m_\pi/2$ that shifted towards larger $\Delta\mu$ with increasing temperature.

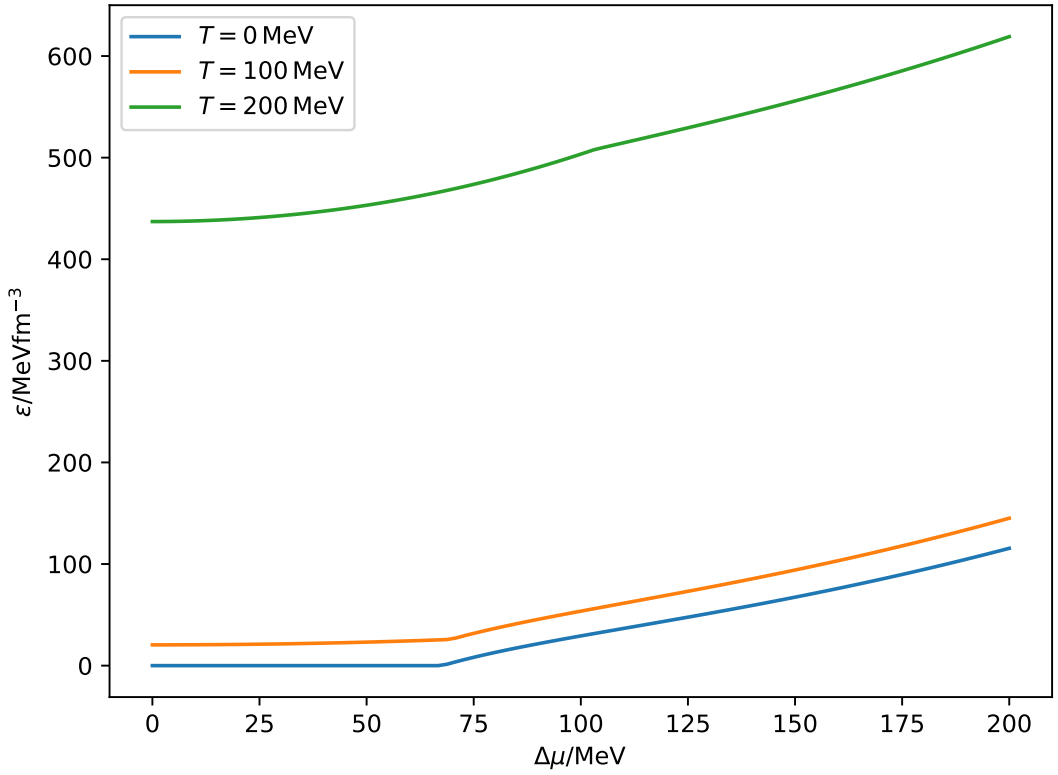

Figure 3.10: Energy density against $\Delta\mu$ at different T

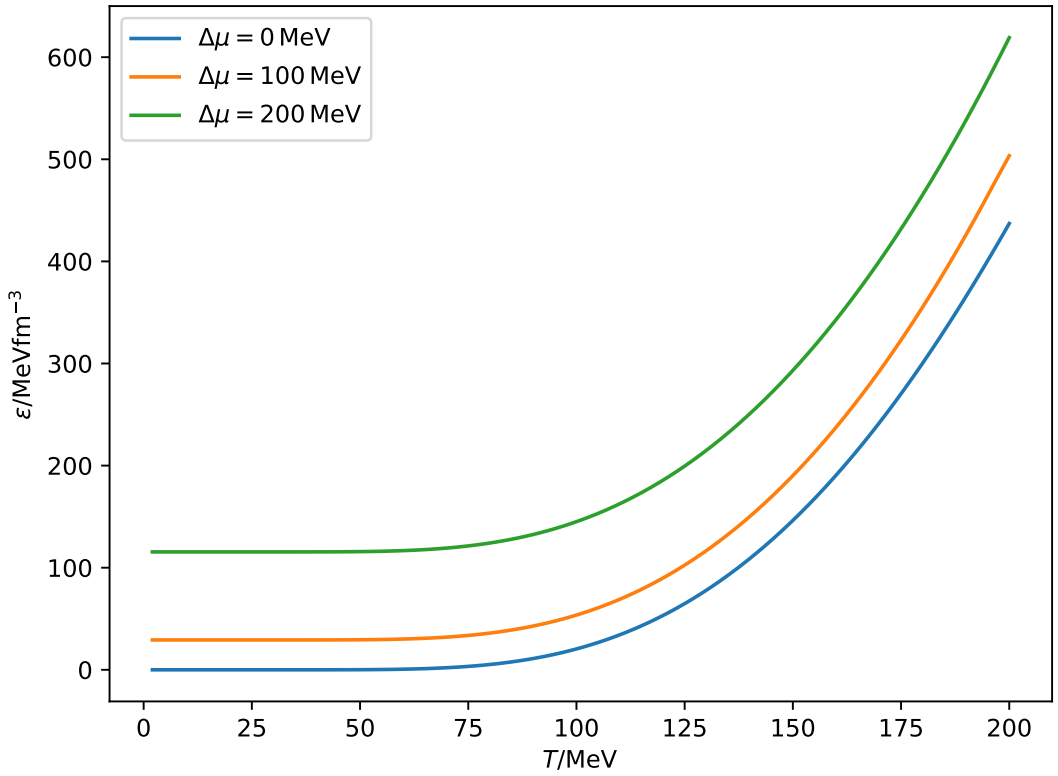

Figure 3.11: Energy density against T at different $\Delta\mu$

4 Comparison with literature results

4.1 Vanishing temperature

In this section we compare our results with those in [3]. There chiral perturbation theory is used at zero temperature. The equation of state they obtained at leading order is a relation between energy and pressure,

$$\epsilon_{LO} = 2\sqrt{p(2f_\pi^2 m_\pi^2 + p)} - p \ ,$$

depending on the pion mass m_π and the pion decay constant f_π. We use the same values for $m_\pi = 135\,\mathrm{MeV}$ and $f_\pi = 92.4\,\mathrm{MeV}$ as in section 3.1, to compare this relation with our results. In [3] different values for m_π and f_π have been used. This way we obtain the pressure energy dependence shown in figure 4.1. Our own results are also plotted there. Different points on these curves correspond to different isospin chemical potential $0\,\mathrm{MeV} \leq \Delta\mu \leq 350\,\mathrm{MeV}$, all at $T = 0$. Up to an energy density of about $\epsilon = 70\,\mathrm{MeVfm}^{-3}$ both results agree. From there they start to diverge. This might be due to the use of different models. It may also point to the missing orders in the chiral perturbation approach or the use of the mean field approximation. Another relation given in [3] is the energy density dependence on $\Delta\mu$ at $T = 0$ in leading order chiral perturbation theory.

$$\epsilon_{LO} = 2f_\pi^2 \Delta\mu^2 \left(1 + \frac{m_\pi^2}{2\Delta\mu^2} - \frac{3m_\pi^4}{16\Delta\mu^4}\right) ,$$

where the same values for m_π and f_π as above have been used. The comparison of this result with our calculations in the Nambu–Jona-Lasinio model is shown in figure 4.2. Here the energy density has been divided by the Stefan-Boltzmann limit $\epsilon_{SB} = 36\Delta\mu/\pi^2$. The results from both models are almost identical.

4.2 Finite temperature

Now we compare our results with the ones from [1]. They use lattice QCD to find the phase transition for the pion condensate phase. In figure 4.3 their results are shown, as well as our own. In both models the pion condensate phase at low temperatures starts at $\Delta\mu = m_\pi/2$. At temperatures above 140 MeV, according to the lattice QCD results, the phase transition shifts to higher isospin chemical potential. The results obtained via the Nambu–Jona-Lasinio model predict the start of this shift for larger temperatures around $T = 200\,\mathrm{MeV}$. Unlike at zero temperature there is a large discrepancy between the predictions made by the NJL model and the ones made by QCD. This difference in temperature dependence does not only affect the pion condensate but all thermodynamic quantities that have been calculated in chapter 3. When probing the theory at high temperatures, this implies high energies, as can be seen in figure 3.11. To describe the behavior of a system at high energies, the physics at small distances needs to be known. Since there are no gluons in the NJL model, the physics of short scales is not represented correctly. This is an explanation for the deviation in temperature dependence.

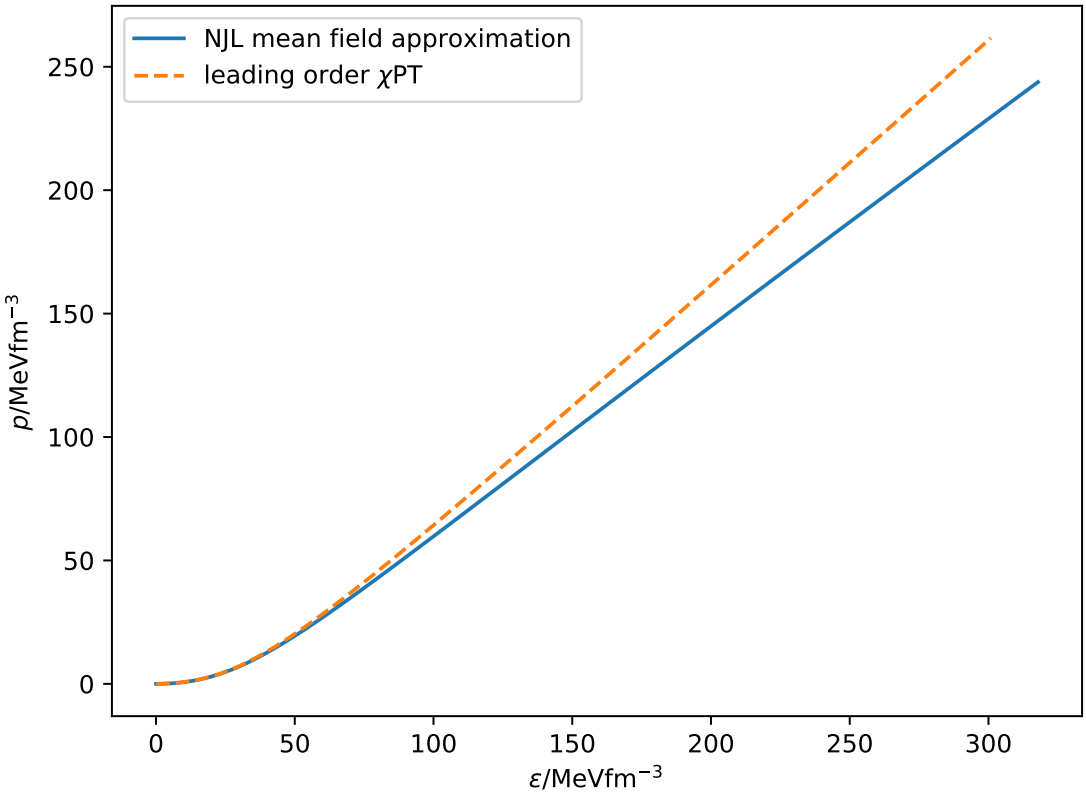

Figure 4.1: Pressure energy dependence at $T = 0$

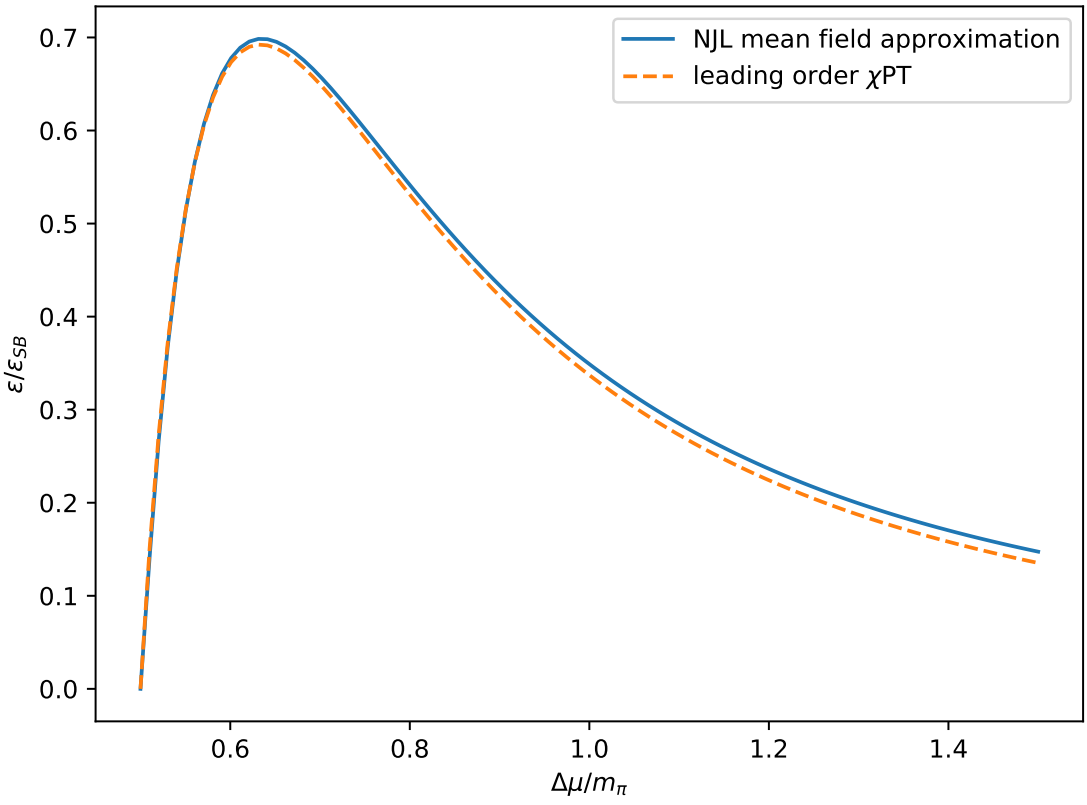

Figure 4.2: Energy divided by the Stefan-Boltzmann limit against $\Delta\mu/m_\pi$ at $T = 0$

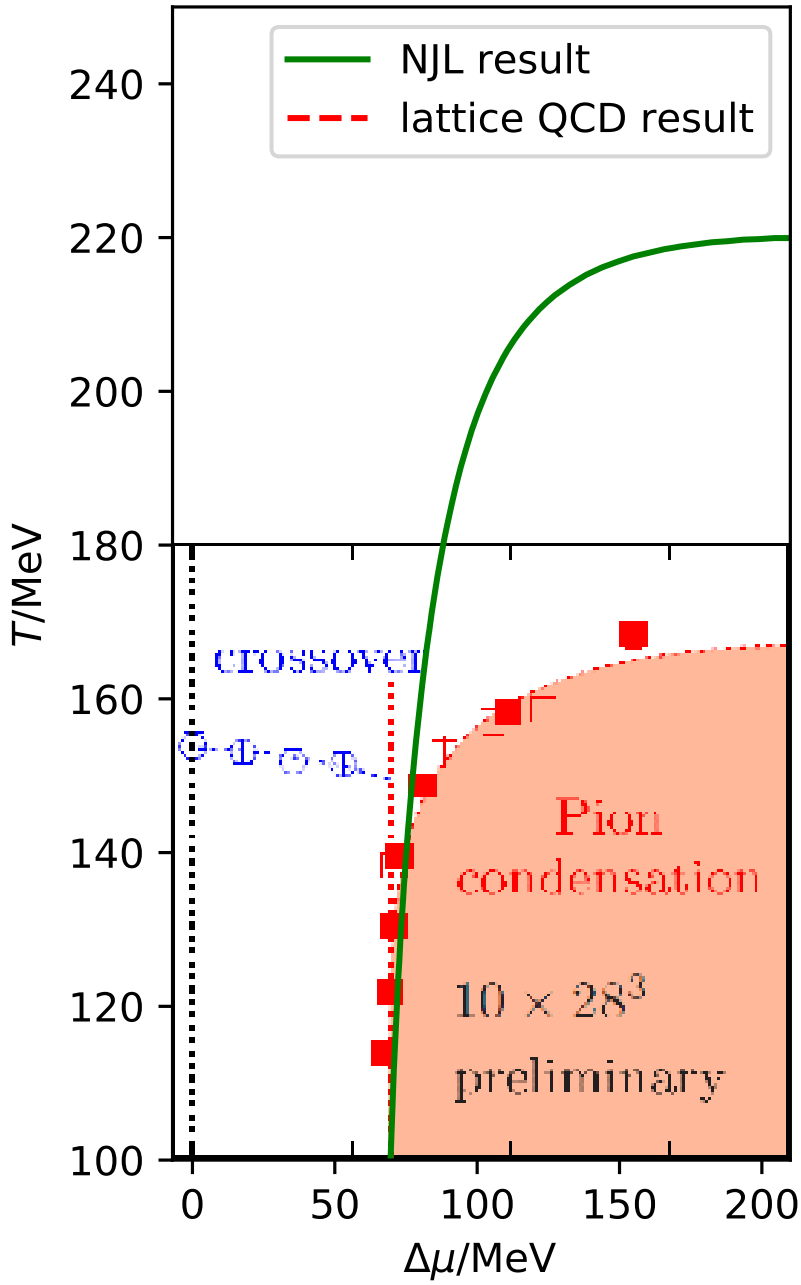

Figure 4.3: Pion condensate phase transition. Our NJL result is plotted in green on top of the lattice QCD result from [1] in red. We do not compare the crossover from lattice QCD in blue to our results.

5 Conclusion

It was the goal to compare predictions made by the Nambu–Jona-Lasinio model with those made by quantum chromodynamics. Therefore we linearized the Lagrangian around the expectation values of sigma and pion condensate. In a next step we used the grand canonical formalism to obtain the gap equation. Its solution gave the condensates dependence on isospin chemical potential and temperature. Then we analyzed the derived thermodynamic quantities pressure, isospin density and energy density. In the end we compared these results with those from previous works. We confirmed the energy pressure dependence predicted by chiral perturbation theory within the scope of the NJL model for low isospin chemical potential. The results for the energy density dependence on isospin chemical potential do also match. That being said, we found out, that the NJL model yields a quantitatively wrong temperature dependence for many observables. Qualitatively these finite temperature results agree with those obtained by lattice QCD calculations. In the future, the discrepancy of the NJL model and QCD at finite temperature could be investigated closer. The NJL model may not yield predictions about reality, but it can serve as a hint and help to advance the insight in strongly interacting matter.

Bibliography

[1] B. B. Brandt, G. Endrodi, and S. Schmalzbauer. QCD at finite isospin chemical potential. *ArXiv e-prints*, September 2017, 1709.10487.

[2] M. Buballa. NJL-model analysis of dense quark matter [review article]. *Phys. Rep.*, 407:205–376, February 2005, hep-ph/0402234.

[3] S. Carignano, A. Mammarella, and M. Mannarelli. Equation of state of imbalanced cold matter from chiral perturbation theory. *Phys. Rev. D*, 93(5):051503, March 2016, 1602.01317.

[4] M. Frank. Das QCD-Phasendiagramm bei endlicher Isospindichte. Diploma thesis, Technische Universität Darmstadt, July 2003.

[5] Y. Nambu and G. Jona-Lasinio. Dynamical model of elementary particles based on an analogy with superconductivity. i. *Phys. Rev.*, 122:345–358, Apr 1961.

[6] K. Rajagopal and F. Wilczek. *The Condensed Matter Physics of QCD*, pages 2061–2151. World Scientific Publishing Co, 2001.